A New Analysis of Oblique Impact Craters on Mars

David Tytell
Division of Geological and Planetary Sciences, California Institute of Technology, Mail Code 170-25, Pasadena, California 91125
tytell@cco.caltech.edu

Stanley G. Love
Jet Propulsion Laboratory, California Institute of Technology, M/S 306-438, 4800 Oak Grove Drive, Pasadena, CA 91109-8099
Stanley.G.Love@jpl.nasa.gov

William F. Bottke, Jr.
Center for Radiophysics and Space Research, Cornell University, Ithaca, NY 14853-6801
bottke@astrosun.tn.cornell.edu

Draft of paper for *Icarus*

July 7, 1998

ABSTRACT

Asteroids or **comets** striking a **planetary surface** at **shallow angles** typically produce **elliptical-shaped craters.** If they have isotropic impact trajectories, the proportion of elliptical craters produced should be proportional to the fraction striking at low angles. Based on laboratory impact experiments, where aluminum or pyrex spheres were shot at high velocities into sand (Gault and Wedekind 1978), it was estimated that less than 1% of all projectiles create elliptical craters. This empirically-derived result, however, disagrees with survey results of the Martian surface, which indicate that approximately 5% of all craters larger than 5 km have elliptical shapes (Schultz and Lutz-Garihan 1982). Thus, if these experimental results are applicable to large craters and the crater survey results are accurate, Mars, at one time, must have had a "special" population of low-angle impactors, perhaps produced by a number of orbitally decaying moonlets similar to Phobos.

To revisit this problem, we tested each part of the hypothesis mentioned above. First, we reexamined the results of two independent Martian crater surveys. Though our results show that elliptical crater identification is somewhat subjective, and that both surveys diverge significantly from one another, we were able to corroborate that roughly 5% of Martian impact craters have major-to-minor axis ratios greater than 1.2. Next, we examined the threshold incidence angle necessary to produce elliptical craters in laboratory impact experiments. Recent results indicate that aluminum targets produce elongated craters at much steeper impact angles than sand targets (Christiansen *et al.* 1993). Interpolating between data produced in sand and aluminum, we derived a new threshold angle for the Martian surface which leads to a predicted proportion of elliptical craters that matches observations within uncertainty (given an ordinary random projectile population). Finally, to test whether Mars was ever hit by a excess number of low-angle projectiles, we numerically modeled the orbital decay of numerous small moons. Our results show a strict correlation between crater size and elongation which is not observed. We conclude that the proportion of elliptical craters on Mars is a natural by-product of projectiles striking at random angles, and that no additional formation mechanisms are needed.

1. Introduction

Impact craters generally appear circular in plain view, even when the projectiles hit from angles substantially off vertical. Though not well understood, this effect is probably caused by hemispherical shape of the projectile's shock wave, which only changes when the impact angle is decidedly oblique (Melosh 1989). Laboratory experiments (small aluminum and pyrex spheres shot at several km/s into sandy targets at various impact angles) indicate that craters are circular down to angles of incidence less than 10° (Gault and Wedekind 1978, hereafter GW78). Below 10°, craters become elongated in the direction of the projectile's flight. The shape of the crater's ejecta blanket in this range are not circular either, but instead take on a "butterfly-wing" shape with the wings perpendicular to the impact trajectory. The extent of a crater's "ellipticity" (ε) can be defined as the ratio between its maximum and minimum rim-to-rim diameter. Craters with $\varepsilon \geq 1.2$ (Fig. 1) have now been observed on all of the terrestrial planets.

Despite their unusual nature, elliptical craters have only been surveyed on Mars. Schultz and Lutz-Garihan (1982) (hereafter SL82) attempted the first such survey by examining craters larger than 5 km for high ellipticity values and for butterfly-wing ejecta patterns. Lunar Planum was found to have a 5% ± 0.4% elongated craters, while Syrtis Major Planitia (3% ± 0.5%) and Uranius Tholus (8% ± 0.4%) all yielded comparable results. Overall, SL82 estimated that ~ 5% of Mars's large craters were substantially elongated.

This outcome, however, is not consistent with values taken from oblique shot experiments into sand targets. GW78 estimated that the threshold angle for producing elongated craters should be 4.75°. Since the probability of an asteroid impacting a given surface at an angle between θ and $\theta + d\theta$ is proportional to $\sin\theta\cos\theta d\theta$, or $\sin^2\theta$, regardless of the target's gravitational field (Shoemaker 1962), the fraction of projectiles striking Mars at $\theta \leq 4.75°$ should only be 0.7%. Thus, the predicted fraction of elliptical craters on Mars is far less than the real fraction (~ 5%).

Three explanations can potentially explain this excess: (i) There are fewer elliptical craters on Mars than claimed by SL82, (ii) The laboratory experiments used to determine the critical angle needed to produce elliptical craters are somehow not applicable to kilometer-sized projectiles (or they have been misinterpreted), or (iii) The excess is real and the crater production population had, for some reason, anisotropic impact angles. If (iii) is correct, it is possible that the elongated crater population on Mars was enhanced by an ancient population of Martian moonlets which conceivably could have spiraled inward under the influence of tidal forces and/or atmospheric drag and struck the planet at very shallow angles (SL82).

To determine which of these possibilities is correct, we carefully examined each in turn. To address (i), we correlated the two existing Martian crater surveys and carried out a new survey ourselves (Sec. 2). To address (ii), we used results of laboratory impact experiments to develop a simple model for predicting the threshold impact angle for producing markedly elliptical craters (Sec. 3, 4). To address (iii), we numerically modeled SL82's "spiraling moonlet" theory, since it provides the best alternative explanation for a pronounced signature of elliptical Martian craters

(Sec. 5). Our final section will discuss our conclusions and future work (Sec. 6).

2. Reexamining Mars's Elongated Crater Population

Since SL82, a second group has independently surveyed the Martian crater population (Barlow 1988, hereafter B88). To develop an updated estimate of the number of elongated craters on Mars, we decided to first compare each group's survey results.

SL82 identified 176 craters larger than 2 km in minimum diameter with ellipticities $\varepsilon \geq 1.1$. They surveyed between Martian latitudes $\pm 65°$. B88 identified 212 craters larger than 2 km with $\varepsilon \geq 1.2$. They surveyed between Martian latitudes $75°$ and $-75°$. Out of these 388 total catalogued craters, only 42 overlapped across the both lists. The overlapping craters tended to have large ellipticities and/or sharp features, unlike the rest of the craters, many of which were quite eroded.

Because of the large discrepancies between the two data sets, and because identifying marginally elliptical craters can be a difficult and subjective process, we decided to make an careful reexamination of all the listed craters. Our new survey took advantage of the on-line Mars Multi-Scale Map (http://www.c3.lanl.gov/~cjhamil/Browse/mars.html), which contains Viking images between latitudes of $\pm 47.5°$. This area encompassed 90% of the listed craters. An examination of a representative sample of impact craters from hardcopy images above $47.5°$ and below $-47.5°$ showed many were significantly eroded, probably due to the periodic expansion and contraction of the Martian polar caps. If elongated craters exist in the region, we doubt that we could conclusively determine they were formed by oblique impact. We therefore ignore these craters in this study. The images retrieved from the Mars Multi-Scale Map have a resolution of 256 pixels/degree.

Elongated craters can be formed by mechanisms other than oblique impact. Examples include: post impact crater wall collapse, sliding debris from impact, and expansion due to faulting. For this reason, we have carefully reexamined each of the 388 elongated craters in our sample using various criteria including ground failure, degree of erosion, crater ellipticity, shape of ejecta blanket, and image quality. The craters were subjectively grouped into four broad categories: "Likely", "Possible", "Unlikely", and "Omitted". We describe these categories below:

Likely. The characteristics of our likely craters are (a) $\varepsilon \geq 1.2$, (b) little to no apparent erosional effects, (c) possible central ridge, and (d) butterfly ejecta blanket. Characteristic (d) is not seen in every crater in this category, but laboratory experiments have shown that it is indicative of impacts which occur at oblique angles (GW78). Fig. 2 is such an example (SL82 crater no. 107). Note its elliptical shape, the clear central ridge, and its ejecta "wings".

Possible. The characteristics of possible craters are (a) $\varepsilon \geq 1.2$, (b) minor to medium levels of suspected erosion, (c) suspected post crater excavation modifications (i.e., faulting, or crater

wall collapse), and (d) poor image quality. We have classified Fig. 3 (B88 crater no. 107) as a possible crater. Though the object appears to be elongated, it lies too close to a region of extreme ground failure. There is no evidence proving or disproving that erosional effects in the region affected this crater.

Unlikely. The characteristics of unlikely craters are (a) $\varepsilon \leq 1.2$, (b) high levels of suspected erosion, (c) other mechanism than oblique impact suspected (i.e., doublet craters, or crater chains), (d) the available image of the region was of poor quality. Erosion was the most frequent reason craters were placed in this group. Fig. 4 (SL82 crater no. 40) is an example where faulting has occurred in the region, thus stretching a once round crater (Thomas and Allemand 1993).

Omitted. Craters were omitted when (a) we were unable to locate them at the referenced location, (b) they were located outside our latitude limitations, or (c) they were indistinguishable from surrounding circular craters in the field (i.e., the image given to us by the Mars Multi-Scale Map was taken from a oblique angle, such that all of the craters in the field look elliptical). The last effect most often occurred at high or low latitudes.

The results of our survey and reanalysis is as follows. Of the 346 total craters (excluding overlaps), 116 were "Likely", 138 were "Possible", 18 were "Unlikely", and 74 craters were "Omitted." Thus, 254 out of 346 craters could be classified as "Likely" or "Possible", an increase of 9% from the B88 survey and an increase of 32% from the SL82 survey. Fig. 5 shows the ellipticity of these craters plotted against their minimum diameter. The mean ellipticity ε of the "Likely" craters is 1.58 ± 0.48, while that of the "Possible" craters is 1.61 ± 0.58. Median ε are 1.50 and 1.47, respectively.

These increases only slightly modify the overall proportion of km-sized elongated craters on Mars. Using SL82 survey numbers, 176 craters encompassed $\sim 5\%$ of Mars's total crater count. Extending this value to our new survey results, we find this value increasing to $\sim 6.5\%$. Therefore, despite the high number of omitted or unlikely craters, the remaining population (between 5-7%) was consistent with the estimates of SL82 and B88. For this reason, we believe the crater surveys themselves can not explain the difference between the Martian elliptical crater population and experimental predictions. Some other factor (or factors) must be responsible.

3. Crater Sizes on Different Planets: Estimates from Scaling Laws

It is possible that the physical parameters of Mars are so different from other planetary bodies that crater formation might be radically different. To check these hypotheses, we will first investigate whether projectiles hitting the Earth, Moon, and Mars make different size craters. We will then look for connections between crater size, ellipticity, and impact angle.

3.1. Pi-Group Scaling Laws

The diameter of a crater on a planet produced by an impacting comet or asteroid is a function of many factors: projectile diameter, target strength, projectile and target densities, impact velocity, and target gravity (Melosh 1989). Large impact events occur infrequently, therefore high-velocity shot experiments are often used to estimate what size projectile created a given crater. In the laboratory, impact geometry as well as target and projectile properties can be controlled effectively. Scaling laws derived from these experiments, though imprecise, allow for interpretation of the crater records of planetary surfaces in a systematic manner.

Currently, pi-group scaling laws yield the best fit relationship between laboratory impact experiments and craters created by buried nuclear weapons (Melosh 1989). This technique has successfully been used to compare craters with similar dimensionless parameters, even though the given impact events themselves had differing velocities, sizes, gravitational accelerations, and target strengths. Pi-group scaling combines the physically relevant parameters in an impact-crater event, such as transient crater diameter D_{at}, impact velocity V, target and projectile densities ρ_{t} and ρ_{p}, target strength Y, planetary gravity g, and projectile mass M into a number of dimensionless ratios which can be measured experimentally. The functional dependence of these values can then be determined by keeping all but the parameters of interest constant.

This procedure is simplified considerably if one assumes that that the target and projectile densities are the same, the projectile is spherical, and that the craters are formed in the gravity regime. The transient crater diameter can then be estimated using the following relation:

$$\pi_D = C_D \pi_2^{-\beta}, \tag{1}$$

with

$$\pi_D = D_{\mathrm{at}} \left(\frac{\rho_{\mathrm{t}}}{M} \right) \tag{2}$$

and

$$\pi_2 = \frac{1.61 g d_{\mathrm{p}}}{V^2}. \tag{3}$$

d_{p} is the diameter of the projectile, while C_D and β are experimentally determined constants, which, for a target of competent rock or saturated soil, are 1.6 and 0.22, respectively. By substituting into (1) and reorganizing, the transient crater diameter relation (D_{at}) is:

$$D_{\mathrm{at}} = \left(\frac{M}{\rho_{\mathrm{t}}} \right)^{1/3} \left(\frac{1.61 g d_{\mathrm{p}}}{V^2} \right)^{-\beta}. \tag{4}$$

This equation is appropriate for impactors striking from a direction perpendicular to a planetary surface.

3.2. Crater Diameters on the Terrestrial Planets

Using (4), we can determine the ratio of crater to diameters for asteroids hitting competent rock or saturated soil on Earth. We estimate that a 1 km asteroid, with a density of 2500 kg m^{-3}, striking at a typical impact velocity of 17 km s^{-1} (Bottke *et al.* 1994), should create a transient crater roughly 10 km in diameter.

We can obtain similar values for the Moon and Mars after varying the different typical impact speeds of asteroids (13 and 12 km s^{-1}, respectively; Bottke *et al.* 1994), and different accelerations for gravity (1.62 and 3.69 m s^{-2}, respectively). The same projectile striking the Moon should produce craters 20% larger than those on Earth, while a comparable impactor striking Mars or Earth would produce roughly identically sized craters. Changing the size of the projectile do not significantly modify these relationships.

We believe that these values are too similar to explain any overabundance of elongated craters on Mars solely using its physical parameters. Therefore, we now reinvestigate the threshold angle assumed to create an elongated crater, as well as the laboratory shot experiments used to determine that result.

4. A Simple Model Relating Impact and Crater Geometries

The dependence of crater ellipticity on projectile impact angle has been found by analogy with hyper-velocity impact experiments into sand targets (GW78), where markedly elliptical craters occur only at impact angles ≤ 4.75 degrees from horizontal. That result forms the basis for the apparent excess of elongated craters on Mars, but it suffers from uncertainty in scaling laboratory results to planetary craters. To reduce that uncertainty, we have developed a relationship between impact angle and crater ellipticity based on observations of experimental craters, and apply it to Mars. It must be noted, however, that at the time of the SL82, GW78 was the only available datum.

4.1. "Line Charges" and the Formation of Elliptical Craters

The first part of our simple model makes use of the semi-quantitative impact-explosion analogy (e.g., Melosh 1989), in which the projectile is treated as an explosive charge. The explosion digs a circular crater many times larger than the projectile, so it can often approximated as a point source.

To model the formation of an elongated crater, we envision the oblique impact as a linear explosive charge which excavates an elongated trench. The ellipticity ε of the trench is determined by the length of the line charge (L) in relation to the size of the final crater (D_c). In the limiting case where $L << D_c$, the line charge can be approximated as a point source producing a near-circular crater with $\varepsilon \rightarrow 1$. In the other extreme ($L$ comparable to D_c; imagine the crater made by a km-long, cm-wide stick of dynamite), $\varepsilon \rightarrow \infty$.

The following thought experiment helps clarify this issue. Imagine that a 10 m "bomb" is capable of making a circular crater 100 m across. Thus, each point on the crater rim is only 45 feet from the edge of the bomb. Now, suppose we reshaped the bomb into a 10×20 m ellipse with the same explosive power as before (i.e., the new bomb is analogous to the "line charge" discussed above). When the elongated bomb explodes, it still makes a crater with a rim 45 m from the edge of the bomb. Accordingly, the minor axis of the crater is still 100 m, but the major axis is now 45 m + 20 m (the long axis of the bomb) + 45 m = 110 m ($\varepsilon = 1.1$). Thus, stretching the bomb out by a factor of 2 only served to increase the long axis of the crater by 10%.

Use of a stronger bomb or weaker dirt lowers the crater's ellipticity. For example, if our 10 m bomb were now to make a 200 m crater, with the bomb edge to crater rim being 95 m, our stretched-out bomb would make a crater 200×210 m ($\varepsilon = 1.05$), only a 5% stretch. Conversely, a weaker bomb or stronger dirt increases the crater's ellipticity. If our 10 m bomb were to make a 50 m crater, with the bomb edge to crater rim being 20 m, our stretched-out would yield a crater 50×60 m ($\varepsilon = 1.2$), a 20% stretch. In other words, if the crater produced is only slightly larger than the bomb itself, the bomb can no longer be treated as a point source, and the "shape" of the bomb makes a difference.

We extend this analogy to elongated impact craters by noting that in an oblique impact, the projectile's "footprint" on the target surface is an ellipse with an axis ratio of $1/\sin\theta$, where θ is the impact angle measured from horizontal. (This result follows readily from geometry.) In the impact-explosion analogy for elliptical craters, the elongated projectile footprint is analogous to the linear explosive charge.

Thus, to summarize this counter-intuitive result, the larger the ratio of crater size (D_c) to projectile size (D_p), the more difficult it is to create elliptical craters. This rule-of-thumb is very useful in interpreting the laboratory experimental data described below.

4.2. Experimental Data on Oblique Impacts

The second part of our simple model draws upon measurements of experimental oblique impact craters drawn from the literature. GW78 and Christiansen *et al.* (1993; hereafter C93), carried out oblique impact experiments using sand and aluminum targets respectively. Their results (crater elongation as a function of impact angle, measured from horizontal) are summarized in Fig. 5. As expected, craters are circular at steep angles and become increasingly elongated at

shallow angles. Within uncertainty, the dependence of elongation on impact angle for elliptical craters follows the same $\sim 1/2$ power law in both studies. There is, however, a significant difference in the threshold angle for producing markedly elliptical craters: 4.75° for GW78 versus 25° for C93. This mismatch reveals that the threshold angle varies dramatically if the conditions of impact are changed and calls into question the assumption that cm-scale laboratory sand targets are an adequate analog for km-scale planetary surfaces.

We now return to the impact-explosion analogy which, as noted above, suggests that crater ellipticity depends on the crater-to-projectile diameter ratio (D_c/D_p). C93 report that, for vertical impacts of aluminum projectiles into aluminum targets at 6.5 to 7.0 km s^{-1}, the crater diameter is ~ 4.7 times the projectile diameter. Gault *et al.* (1974) show a ratio of ~ 61 for the vertical impact of an aluminum projectile striking sand at the 6.4 km s^{-1} speed used by GW78 for their threshold elliptical crater. Craters in sand are thus more than an order of magnitude larger than craters in aluminum caused by identical impactors. It follows from the previous discussion that much shallower impact angles (corresponding to much more elongated projectiles) are needed to produce distorted craters in sand than in aluminum.

Next, we use the dependence of the elliptical crater threshold angle on the normal impact crater-to-projectile diameter ratio to estimate the threshold angle $\theta_{\rm ET}$ (elliptical threshold) for Mars. To do so, we first fit a power-law to the two available pairs of data for crater-to-projectile diameter ratio and threshold angle for elliptical crater production [(4.7, 25), (61, 4.75)]. This technique is used with some trepidation, but it must suffice in the absence of additional appropriate data or theoretical underpinning. The result is:

$$\theta_{\rm ET} = 68.1 \left(\frac{D_c}{D_p} \right)^{-0.648} . \qquad (5)$$

For km-scale asteroids striking Mars with vertically impact velocities near ~ 12 km s^{-1}, pi-group scaling predicts a crater-to-projectile diameter ratio near 15. Inserting that value into (5) yields a threshold angle of 12°. We thus expect that km-scale projectiles striking the Martian surface at angles $\leq 12°$ above the horizon should produce markedly elongated craters ($\varepsilon \geq 1.2$). Assuming the canonical $\sin^2\theta$ probability distribution for random impact angles, we predict that $\sim 4\%$ of Martian craters should be elliptical.

The above result compares favorably with the 5 to 7% of elliptical craters observed by various researchers (SL82, B88, this study) in Martian crater counts, but contrasts strongly with the 0.7% value derived solely from the GW78 data. Thus, our analysis suggests that there is no overabundance of elliptical craters on Mars, and obviates the need for an exotic mechanism to explain them.

5. A Test of the Spiraling Moonlet Hypothesis

We now address the other remaining plausible theory capable of explaining the overabundance of craters on Mars. SL82 proposed that ancient satellites lying in Mars's equatorial plane could have spiraled inward and impacted Mars at oblique angles, thereby causing the apparent excess of elliptical craters on Mars. They supported this hypothesis by suggesting that many of Mars's elliptical craters lie along great circles. Different circles were, presumably, caused by polar wander. The satellites themselves, of which Phobos and Deimos are the last remaining survivors, decayed inward by gas drag, caused by an extended early Martian atmosphere, or by tidal drag. The latter effect is supported by Phobos itself, which is tidally decaying rapidly enough that it will collide with Mars over the next 40 Myr (Burns 1992).

As a preliminary check of this hypothesis, we have plotted the location and crater orientation of each of the 254 "Likely" and "Possible" craters elliptical described in Fig. 5 on a orthographic projection of Mars (Fig. 6). The vectors are given a length proportional to their ellipticity ε. Since most craters have $\varepsilon \sim 1$, most vectors are similar in size. The crater's latitude and longitude corresponds to the center of the vector. Presumably, if the dominant mechanism producing these craters were orbital decay, many of these vectors would intersect and be aligned with one or more imaginary planes passing through the surface and center of Mars. Though we have not attempted to model this testing technique, a qualitative examination of Fig. 6 reveals few conspicuous vector alignments, suggesting the spiraling moonlet scenario is possibly a contributing but not a dominating effect. SL82, who were more quantitative, came to a different conclusion. The resolution of this discrepancy is left for future work.

To more rigorously evaluate the spiraling moonlet scenario, we speculated about the "fingerprints" such a process would leave behind on the Martian surface. When Phobos-like moonlets enter Mars's atmosphere, aerodynamic drag should cause them to spiral inward until they impact the surface (if they stay intact). We hypothesize that larger moonlets, which are less susceptible to aerodynamic drag, should strike at more oblique angles that smaller moonlets. Thus, a correlation between crater size and ellipticity should be evident in the resulting crater population.

Our test of the spiraling moonlet scenario consists of three steps. In the first step, we track the evolution and impact trajectories of moonlets of various sizes in Mars's early atmosphere (Sec. 5.1). Next, we relate impact angle to crater ellipticity for each moonlet using pi-group scaling theory (Sec. 5.2). In the third step, we find the minor diameter ($D_{\min}$) of each crater, so that the model results can be compared with measurements.

5.1. Modeling the Orbital Decay and Impact of Spiraling Moonlets

5.1.1. Equations of Motion for Atmospheric Entry

To track the the evolution and impact trajectory of moonlets of various sizes in Mars's early atmosphere, we integrate the equations of motion for atmosphere entry (e.g., Passey and Melosh 1980; Love and Brownlee 1991). We briefly review them here.

Upon entering an atmosphere, air molecules strike a projectile (assumed to be spherical), slowing it down, heating it, and reorienting its impact trajectory towards the planetary surface. A bow shock forms in front of the projectile, and the gas pressure there is:

$$P = \rho_{\rm atm} v^2, \tag{6}$$

where $\rho_{\rm atm}$ is the density of the atmosphere and v is the velocity of the projectile. The pressure behind the projectile is zero. The drag force on the projectile can be written as:

$$\mathbf{F}_{\rm drag} = \mathbf{P}A = \rho_{\rm atm} A v^2 \hat{v} \tag{7}$$

where A is the cross-sectional area of the projectile. The momentum change in a small time step dt is equal to the mass encountered times the relative velocity, plus a gravitational term:

$$d\mathbf{p} = \left(m\mathbf{g} - C_{\rm drag}\, \rho_{\rm atm}\, v^2 \hat{v} \right) \tag{8}$$

where $C_{\rm drag}$ is a drag coefficient which, for asteroid-size bodies, we set to 1. Expressing (8) in terms of v, we get:

$$d\mathbf{v} = \left(\mathbf{g} - C_{\rm drag} \frac{\rho_{\rm atm} v^2}{\rho_{\rm p} r} \hat{v} \right) dt \tag{9}$$

where the spherical projectile's radius r and density $\rho_{\rm p}$ are now shown.

We integrate (9) using a fourth-order Runge-Kutta numerical integrator. The flight of the projectile is two-dimensional so we take into account the curvature of the planet and its atmosphere when calculating the impact trajectory of the projectile. Starting conditions and results are described below.

5.1.2. A Simple Early Martian Atmosphere

If many of the elliptical craters on Mars are more that 3 Gyr old, as claimed by SL82, it is probable they were formed when Mars still had a thick, dense atmosphere (Owen 1992). To

model this early atmosphere in our simulation, and to keep things simple, we assume (i) it was primarily composed of CO_2, much like the current atmosphere, and (ii) that the surface pressure and temperature were high enough to maintain liquid water on the surface ($\sim$ 1 bar and 273 K, respectively). Note that these approximations are not that far from predicted conditions (Fanale *et al.* 1992). Using these values, we estimate that an early Martian atmosphere would have had a scale height $H = 13.8$ km and a surface atmospheric density $\rho_{\rm atm} = 2.1$ kg m^{-3}. The density of the Martian atmosphere at different altitudes is given by:

$$\rho(z) = \rho_{\rm atm} e^{-(z/H)}, \tag{10}$$

where z is the distance above the planetary surface (Chamberlain and Hunten 1987). (10) can be used in (9) to obtain the drag force on the projectile.

5.1.3. Impact Angles for Spiraling Moonlets

To determine the impact angles for our Martian moonlets of various sizes (200 m to 50 km in diameter), we assume the objects start out on a circular orbit 100 km above the surface. Each spherical moonlet has a density of 2500 kg m^{-3}. Our integration timestep is 10 sec. Smaller timesteps do not change the final result. Objects are integrated until they cross the Mars's surface, where the impact angle in computed.

Our results show, as expected, an inverse correlation of impact angle (measured from the horizontal) with projectile size (Table 1). This relationship is readily understood by considering the bodies' ballistic coefficients: larger moonlets (with a greater ratio of mass to cross-sectional area) are less deflected from their original paths by air drag than are smaller ones. Comparable relationships are expected for different model atmosphere properties.

5.2. Relating Impact Angle to Crater Ellipticity

Our next goal is to find the relationship between impact angle and crater ellipticity ε. To do so, we first estimate the rim-to-rim diameter of the crater made in the vertical impact of a projectile striking Mars at 3.5 km s^{-1} (Mars low circular orbit velocity) using (4). A list of vertical impact crater sizes for various impactor sizes are in Table 1.

The resulting crater-to-projectile diameter ratios are used along with (5) to yield $\theta_{\rm ET}$, the threshold angle for markedly elliptical craters, for each case. Crater ellipticity ε is then derived from the actual impact angle (θ) using relationships analogous to the one illustrated in Fig. 7 for typical Mars impacts. These relations may be expressed as:

$$\varepsilon = \max\left\{1.2\left(\frac{\theta_{\rm ET}}{\theta}\right), 1.0\right\} \tag{11}$$

The results are listed in Table 1; the uncertainty in the numbers is estimated from Fig. 7 at *sim*20%.

5.3. Finding Crater Widths

The third step is to find the minor diameter ($D_{\rm min}$) of each crater, so that the model results can be compared with measurements. C93 show that major diameter grows and minor diameter shrinks with decreasing impact angle (Fig. 8). Because these experiments represent the best available data set on the change of crater geometry with impact angle, we refer to them in this treatment in spite of our earlier argument that the relationships between various cratering parameters that hold for laboratory impacts on aluminum targets may not hold for km-scale craters on Mars. We minimize the effects of size and materials, however, by examining only relative geometrical parameters and avoiding direct reference to the kinetic and material properties of the projectile and target. The C93 data exhibits the following geometrical relationship:

$$D_{\rm min} = CD^{0.625} \tag{12}$$

where C is a constant and all other impact parameters are held constant.

(12) matches the data within 5% if the constant is set equal to the diameter of the crater resulting from a vertical impact. Applying it to Mars craters is equivalent to assuming that the geometrical interrelationships of all elliptical craters are the same, even though it requires different impact angles to make craters of the same ellipticity under different circumstances. Using (12) together with our spiraling moonlet impact geometries, we produce the leftmost column in Table 1. The last two values (corresponding to ellipticity values much larger than the maximum observed) are smaller than the projectile diameter and are probably not meaningful. We estimate a $\sim$ 50upper limit of the uncertainty in each column.

The points defined by the leftmost two columns of Table 1 are plotted in Fig. 9, along with the observed crater population. It shows that outcomes produced by the spiraling moonlet scenario are nothing like observed crater ellipticity relationships. Thus, we can now say, quantitatively, that spiraling moonlets did not produce a significant fraction of elliptical craters on Mars.

6. Conclusions

Our study found that despite discrepancies between catalogued elongated craters lists, the total number of elongated craters represent approximately 6% of the Martian crater population,

which is reasonably close to the abundance measurements of previous studies. Our reevaluation of the threshold angle (θ_{ET}) necessary to produce an elongated crater on Mars, however, implies angles of $\leq 15°$ rather than $\leq 4.75°$ as previously believed. This result is based on laboratory impact data provided by C93, which was unavailable to SL82 at the time of their survey. For that reason, the conclusions of SL82, based solely on the experimental data of GW78, are inaccurate.

Our new value for θ_{ET} yields an expected elongated crater abundance of 4%, which is close to the observed value. Other elliptical crater scenarios (e.g., moonlets crashing as a result of orbital decay), in our opinion, are superfluous, though we can not rule out the possibility that a small fraction of the entire Martian elliptical crater population are made in unusual ways. Tests of the spiraling moonlet hypothesis, however, show a strong correlation between minimum size and ellipticity, which is not seen in the data.

We believe that the results of this study should readily allow us to predict an accurate elongated crater abundance for other heavily impacted bodies, i.e., Venus, Mercury, and the Moon. Future work will analyze these bodies, both by determining the observed number of elongated impacts, and matching those results to theory.

Acknowledgments

We thank Nadine Barlow for her elliptical craters data set, Calvin J. Hamilton of Los Alamos National Laboratory, and the National Space Science Data Center for the use of the Mars Multi-Scale Map. We also thank Jay Melosh and Joe Burns for useful commentary and discussions. This project was supported by David Tytell's SURF (Summer Undergraduate Research Fellowship) grant at Caltech, Stanley G. Love's O. K. Earl Prize Fellowship at Caltech, and William F. Bottke's Texaco Prize Fellowship at Caltech. Additional support was provided by NASA Grant NAGW-310.

REFERENCES

BARLOW, N. G. 1988. Crater size-frequency distributions and a revised Martian relative chronology. *Icarus* **75**, 285–305.

BOTTKE, W. F., M. C. NOLAN, R. GREENBERG, AND R. A. KOLVOORD 1994. Collisional lifetimes and impact statistics of near-Earth asteroids. In *Hazards Due to Comets and Asteroids* (T. Gehrels and M. S. Matthews, Eds.), pp. 337–357. Univ. of Arizona Press, Tucson.

BURNS, J. A. 1992. Contradictory clues as to the origin of the Martian moons. In *Mars* (H. H. Kieffer, B. M. Jakosky, C. W. Snyder, and M.S. Matthews, Ed.), pp. 1257–1282. Univ. of Arizona Press, Tucson.

CHRISTIANSEN E. L., E. D., CYTOWSKI, AND J. ORTEGA 1993. Highly oblique impacts into thick and thin targets. *Int. J. Impact Eng.* **14**, 157–168.

FANALE, F. P., S. E. POSTAWKO, J. B. POLLACK, M. H. CARR, AND R. O. PEPIN 1992. Mars: Epochal climate change and volatile history. In *Mars* (H. H. Kieffer, B. M. Jakosky, C. W. Snyder, and M.S. Matthews, Eds.), pp. 1135–1179. Univ. of Arizona Press, Tucson.

GAULT D. E., F. HÖRZ, D. E. BROWNLEE, AND J. B. HARTUNG 1974. Mixing of the Lunar regolith. *Proc. Lunar. Sci. Conf.* **5**, 2365–2386.

GAULT, D.E., AND J. A. WEDEKIND, 1978. Experimental studies of oblique impacts. *Proc. Lunar. Sci. Conf.* **9**, 3843–3875.

GILBERT G. K. 1893. The moon's face, a study of the origin of its features. *Bull. Philos. Soc. Wash.* **12**, 241–292.

MELOSH, H. J. 1989. *Impact Cratering: A Geologic Process.* Oxford University Press, New York., pp. 117–123.

OWEN, T. 1992. The composition and early history of the atmosphere of Mars. In *Mars* (H. H. Kieffer, B. M. Jakosky, C. W. Snyder, and M.S. Matthews, Ed.), pp. 818–834. Univ. of Arizona Press, Tucson.

THOMAS, P. G., AND P. ALLEMAND 1993. Quantitative analysis of the extensional tectonics of Tharsis Bulge, Mars. Geodynamic implications. *J. Geophys. Res.* **98**, 13097–13108.

SCHULTZ, P. H., AND A. B. LUTZ-GARIHAN 1982. Grazing impacts on Mars: A record of lost satellites. *J. Geophys. Res.* **87**, A84-A96.

SCHULTZ, P. H. AND D. E. GAULT 1985. Clustered impacts: Experiments and implications. *J. Geophys. Res.* **90**, 3701–3732.

SCHULTZ, P. H. AND R. E. LIANZA 1992. Recent grazing impacts on the Earth recorded in the Rio Cuarto crater field, Argentina. *Nature* **355**, 234–237.

SHOEMAKER, E. M. 1962. *Interpretation of lunar craters.* In *Physics and Astronomy of the Moon* (Z. Kopal, Eds.), Academic Press, N.Y., pp. 283–359.

Impact Angles and Crater Ellipticities for Spiraling Moonlets					
Moonlet Diameter (km)	Impact Angle (deg)	Crater Diam. for Vertical Impacts (km)	θ (ET) (deg)	Ellipticity ε	Minor Crater Diameter (km)
0.2	10.4	2.46	14.2	1.6	1.83
0.5	6.9	5.03	16.1	2.8	2.65
1	5.2	8.64	17.7	4.1	3.58
2	4.0	14.8	19.5	5.8	4.95
5	2.8	30.3	22.1	9.5	7.44
10	2.2	52.0	24.3	13.2	10.4
20	1.7	89.3	26.8	18.9	(14.3)
50	1.2	183	30.4	30.4	(21.7)

Table 1: Results from the spiraling moonlet model. The impact angle is calculated when the moonlet strikes the Martian surface. The crater diameter is given by (4). $\theta_{\rm ET}$ is given by (5). ε is given by (11). The minimum diameter of the crater formed is given by (12). The two values in parentheses correspond to crater diameters less than the projectile diameter, indicating (12) is no longer a valid approximation.

Fig. 1.— Martian crater formed by oblique impact. The crater is located at 25° latitude, 97.5° longitude. It is 35 × 18 km in diameter, giving it an ellipticity $\varepsilon = 1.9$. Note its well defined butterfly-wing ejecta pattern and central ridge. The only known mechanism for creating such ejecta patterns is oblique impact. This crater is SL82, no. 37.

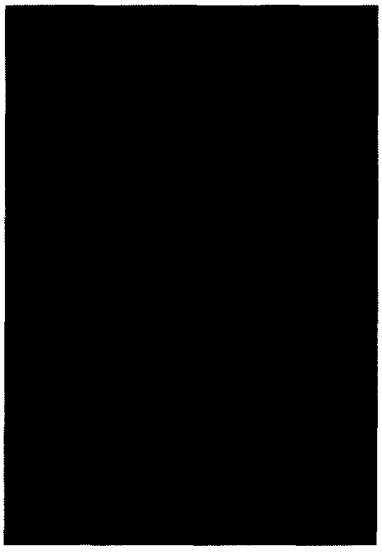

Fig. 2.— "Likely" oblique impact crater located at $-18°$ latitude, $72°$ longitude. Its dimensions are 18×15 km, yielding $\varepsilon = 1.2$. Note the strong butterfly-wing ejecta blanket just like that seen in Fig. 1. This crater is SL82, no. 107.

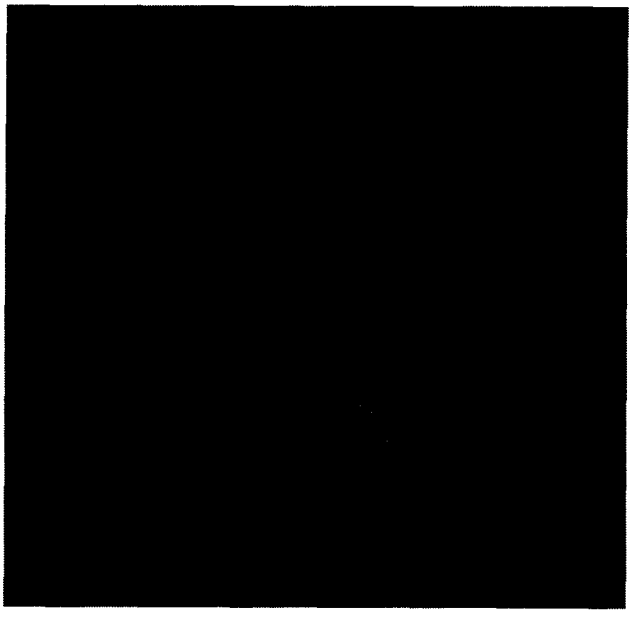

Fig. 3.— "Possible" oblique impact crater located at $-12°$ latitude, 48° longitude. Its dimensions are 17×13 km, yielding $\varepsilon = 1.4$. Since part of the crater is truncated by the canyon, we do not classify it as "Likely". This crater is B88, no. 107

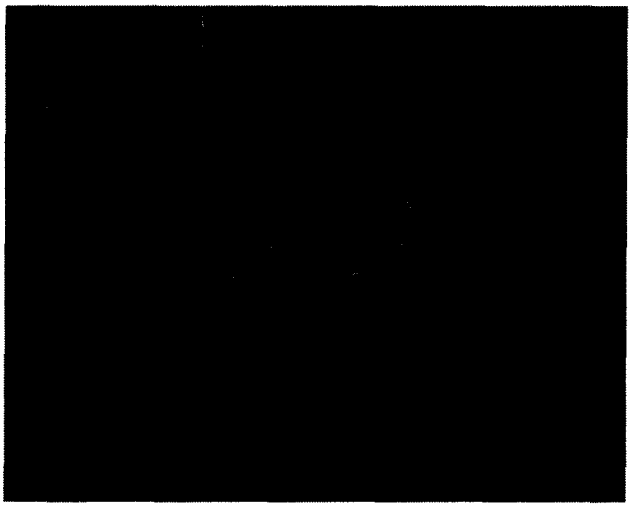

Fig. 4.— "Unlikely" oblique impact crater located at 29° latitude, 82° longitude. Its dimensions are 30 × 10 km, yielding $\varepsilon = 3.0$. This image has been was used by Thomas and Allemand (1993) to demonstrate how faulting can increase crater elongation. This crater is SL82, no. 40.

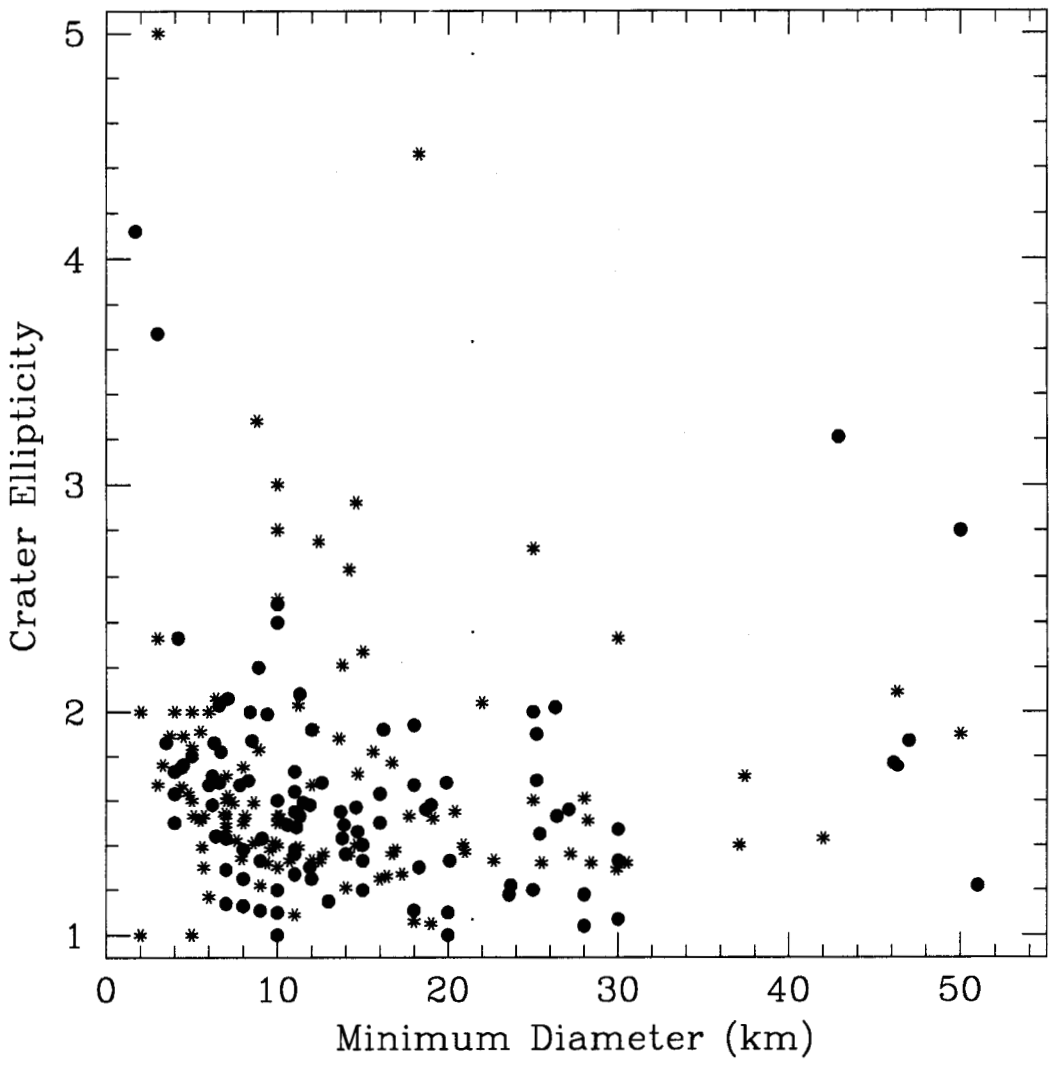

Fig. 5.— Minimum crater diameter (km) plotted against ellipticity (ratio of maximum and minimum crater diameters) for 116 "Likely" craters (solid circles) and 139 "Possible" craters (stars).

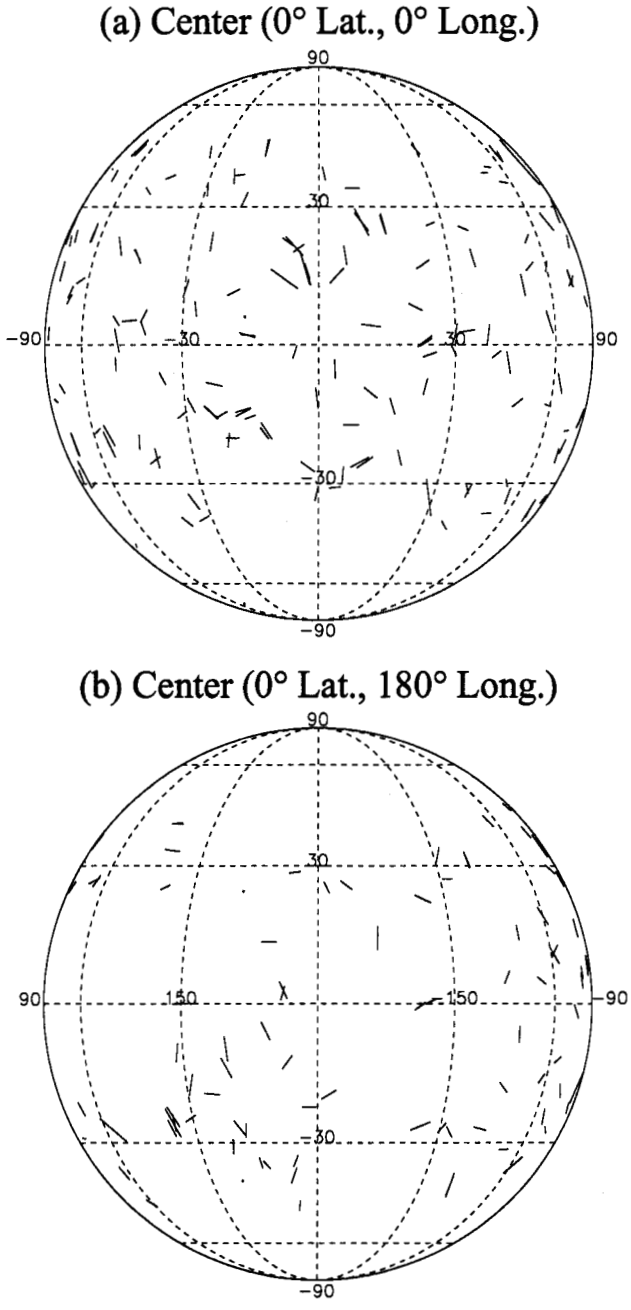

Fig. 6.— The location and crater orientation for each of the 254 "Likely" and "Possible" craters elliptical described in Fig. 5. The vectors are given a relative length proportional to their ellipticity ε. The crater's latitude and longitude corresponds to the center of the vector. (a) The center of the orthographic projection is 0° latitude and 0° longitude. (b) The center of the orthographic projection is 0° latitude and 180° longitude.

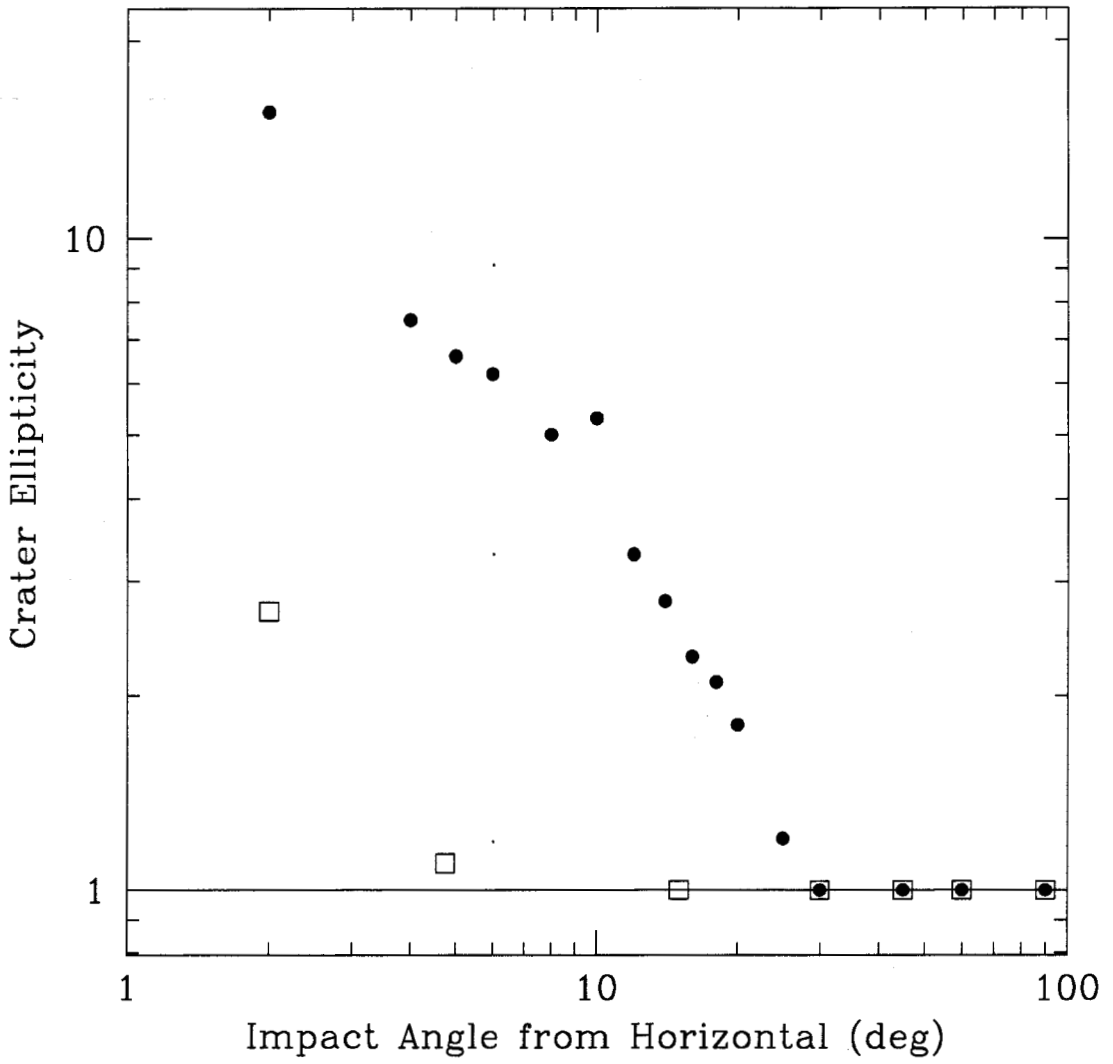

Fig. 7.— Crater ellipticity vs. impact angle, plotted for the laboratory impact experiments of GW78 (open squares) and C93 (solid circles). GW78 fired aluminum and pyrex spheres into sand targets at 6.4 km s^{-1}, while C93 fired aluminum spheres into aluminum targets at 6.5–7.0 km s^{-1}.

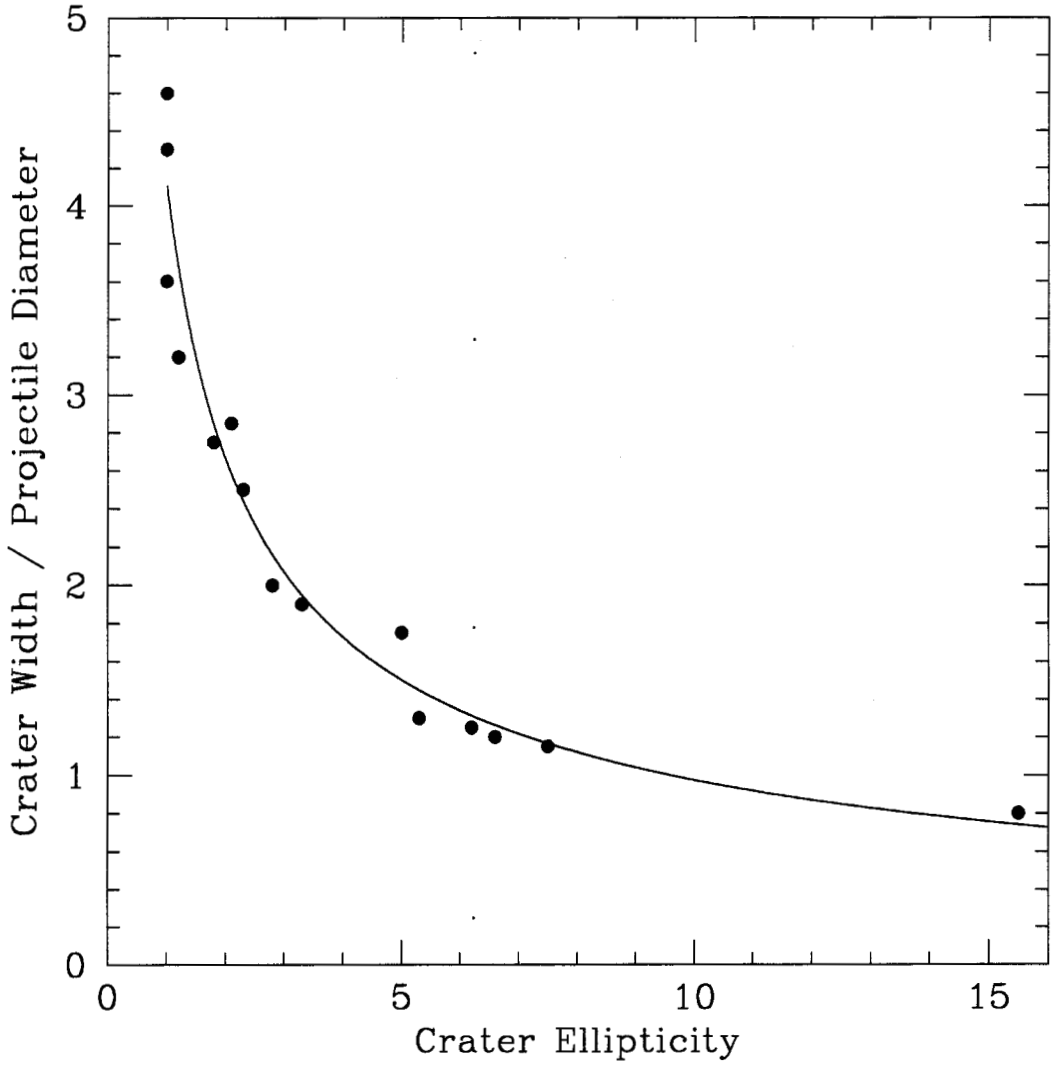

Fig. 8.— The minimum diameter, or width, of each crater from C93 is scaled by the projectile's diameter and plotted against the crater's ellipticity ε. The solid curve was found using a least squares fit method. It has the functional form $y = 4.1062x^{-0.6247}$.

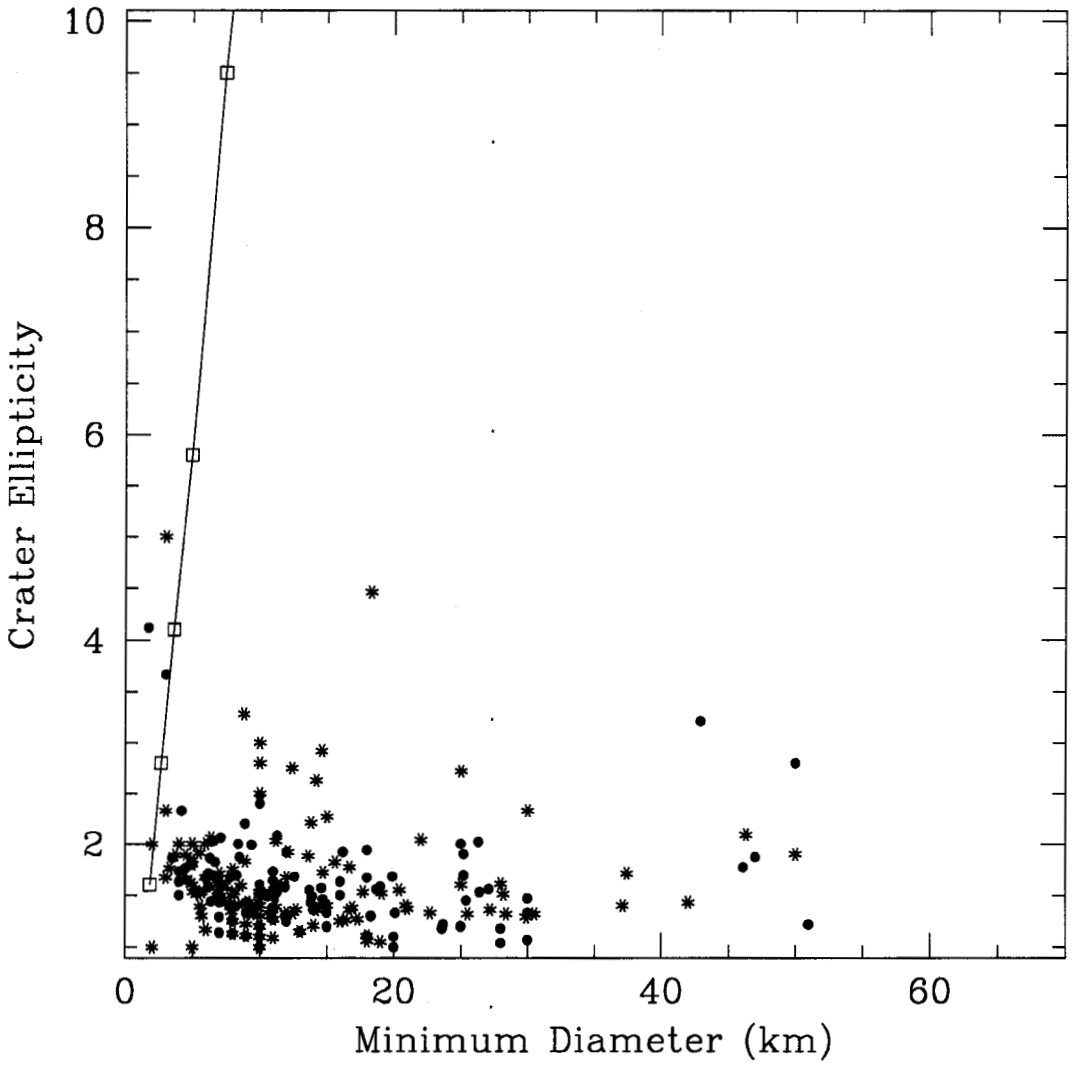

Fig. 9.— The results from the Martian "spiraling moonlet"orbital decay hypothesis (Table 1; open squares) are ploted against the Martian crater data shown in Fig. 5. The mismatch between the model results and the data is apparent, suggesting that few elliptical craters on Mars were produced by this mechanism.